Mobile Cryocooler-Based SQUID NDE System Utilizing Active Magnetic Shielding

Yoshimi Hatsukade, Tomohiro Inaba, Yoshio Maruno, and Saburo Tanaka

Abstract—**A mobile cryocooler-based SQUID NDE system was developed for realization of NDE of fixed targets that can't be moved or rotated. In order to move the SQUID in an ambient field, an active magnetic shielding technique employing a compensation coil and feedback circuit including a band elimination filter was introduced in a SQUID NDE system. The HTS SQUID gradiometer was cooled by a coaxial pulse tube cryocooler to 74 K ± 0.04 K. The flux noise caused by moving the SQUID at 32 mm/s was well suppressed. Unlocking of the flux-locked loop (FLL) circuit or a significant increase in noise did not occur during the motion. Detection of hidden slots in fixed single and double-layered carbon/carbon composites in ambient field was demonstrated by moving the HTS SQUID gradiometer.**

Index Terms—**Active magnetic shielding, carbon-fiber composites, cryocooler, mobile, SQUID NDE.**

I. Introduction

In THE last decade of the 20th century, significant research using SQUID NDE focused on aircraft structures, such as multilayered aluminum plates (some with rivets), wheels, and engine turbine blades [1]–[4]. In addition to the metallic objects, recent work was extended its application to carbon-fiber composites, which are increasingly being employed by aircraft and aerospace manufacturers [5]–[8]. The SQUID NDE technique is now recognized as an emerging NDE technology. However, improvements are still needed to ensure widespread industrial use [9].

So far, almost every specimen tested with a SQUID was inspected while fixing the sensor and moving or rotating the specimen, with some exceptions [2], [10], [11]. However, in actual practice, large-scale structures usually can't be moved or rotated for inspection. In such situations, a mobile NDE system is indispensable. Applying a cryocooler to such a system may simplify operation.

In this study, an active magnetic shielding technique, employing a simple compensation coil and feedback circuit, was developed so that the sensor can be moved without unlocking or increasing noise. With this technique, we constructed a mobile cryocooler-based SQUID NDE system, which could move an HTS SQUID gradiometer in an ambient field near stationary specimens. Detection of hidden slots in single and multilayered carbon/carbon composites (C/C) was demonstrated for investigating the performance of the system.

Manuscript received October 4, 2004; revised January 6, 2005. This work was supported in part by The 21th Century COE Program "Ecological Engineering for Homeostatic Human Activities," from the ministry of Education, Culture, Sports, Science and Technology.

Y. Hatsukade, T. Inaba, and S. Tanaka are with the Toyohashi University of Technology, Toyohashi, Aichi 441-8580, Japan (e-mail: hatukade@eco.tut.ac.jp; ew023804@mail.eco.tut.ac.jp; tanakas@eco.tut.ac.jp).

Y. Maruno is with Iwatani Industrial Gases Corporation, Shiga 524-0041, Japan (e-mail: maru@iig.iwatani.co.jp).

Digital Object Identifier 10.1109/TASC.2005.850026

II. Sensor-Mobile SQUID-NDE System

A. System Schema

The mobile SQUID NDE system constructed in this study is comprised of the following: an HTS SQUID gradiometer, electronics, coaxial pulse-tube cryocooler (PTC), cryostat, temperature controller, electric XY scanner, motor controllers, metallic arm, personal computer (PC), function generator, lock-in amplifier, compensation coil, band elimination filter (BEF), attenuator and eddy-current inducer. A schematic sketch of the system is shown in Fig. 1(a). Fig. 1(b) shows a photograph of the cryostat integrated with the cryocooler, aluminum arm and XY scanner. The eddy-current inducer was placed around the bottom of the cryostat. A specimen was mounted beneath the cryostat.

B. Sensor Details

A planar high-T_c SQUID gradiometer fabricated in our laboratory was employed for use in the ambient field. The gradiometer is also suitable for reduction of magnetic noise caused by the mechanical vibration of the cryocooler. A $SrTiO_3$ bicrystal substrate with mis-orientation angle of 30° was used. A $YBa_2Cu_3O_{7-\delta}$ thin film with thickness of about 200 nm was deposited on the substrate. The differential pickup coil, composed of two rectangular coils with an area of 3.6 mm × 2.9 mm was connected directly to the SQUID ring. The modulation coil was attached on one side of the pickup coils. Fig. 2 shows the schematic drawing of the HTS SQUID gradiometer. The magnetic flux sensitivity of the gradiometer was about 200 $\mu\phi_0/\mathrm{Hz}^{1/2}$ with flux-locked loop (FLL) operation and liquid-nitrogen cooling in ambient field. The corresponding field gradient sensitivity of the gradiometer was found to be about 22 $\mathrm{pT/cm/Hz}^{1/2}$. The characteristics of the HTS SQUID gradiometer are summarized in Table I.

C. Coaxial PTC and Cryostat

A compact and transportable coaxial PTC was developed for the mobile sensor system. In order to suppress the increase of magnetic noise, the cryocooler and cryostat were made of nonmagnetic materials, such as aluminum, copper, stainless steel and polymeric materials. Because the compressor and rotary valve generated magnetic noise, they were spatially separated from the cryostat by lengths of a few meters. In order to move the cryostat freely, the PTC and rotary valve were connected with a flexible bellows (instead of the usual copper tubing), through

1051-8223/$20.00 © 2005 IEEE

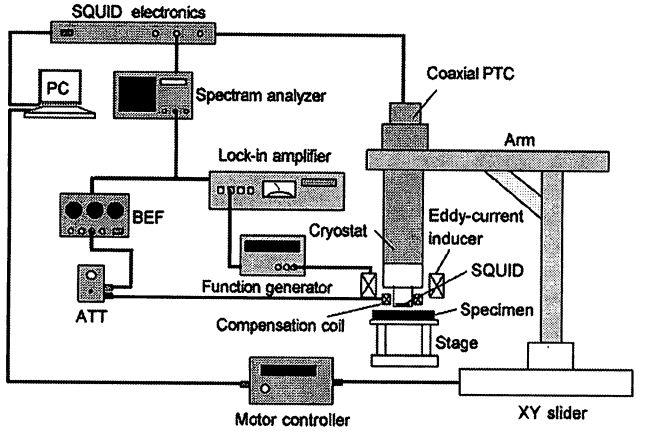

Fig. 1. Mobile SQUID NDE system. (a) Schematic diagram. (b) Photograph of the PTC and cryostat fixed with the aluminum arm on the XY scanner. The PTC is controlled by the XY scanner. The current inducer was placed around the bottom of the cryostat. The specimen on the stage was fixed below the cryostat.

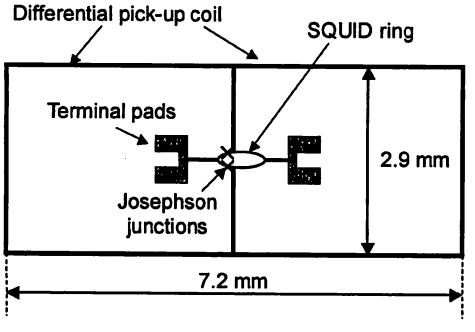

Fig. 2. Schematic drawing of the first-order HTS SQUID gradiometer. The differential pickup coils were directly coupled with the SQUID placed in the center.

which the cooling agent (helium gas) was transmitted between the PTC and rotary valve. The pressure oscillation frequency generated by means of the motor-driven rotary valve was 2.4 Hz. The characteristics of the PTC are summarized in Table II.

For further reduction of the vibration transmitted to the SQUID from the cryocooler and to keep the SQUID away from the possibly magnetized pulse tube (due to welding), an

TABLE I
CHARACTERISTICS OF THE HTS SQUID GRADIOMETER

Items	Characteristics
Substrate	STO bicrystal (30 degree mis-orientation)
Superconductor film	YBCO (200nm in thickness)
SQUID inductance	50 pH
SQUID type	Direct coupled type first-order gradiometer
Pickup coil size	3.6 mm x 2.9mm
Baseline length	3.6 mm
Flux sensitivity	200 $\mu\Phi_0/Hz^{1/2}$ (in LN_2 and ambient field)
Field gradient sensitivity	22pT/cm/$Hz^{1/2}$ (in LN_2 and ambient field)

TABLE II
CHARACTERISTICS OF THE COAXIAL PTC

Items	Characteristics
Cooling capacity	8 W (60Hz at 77 K)
Ultimate temperature	53 K (60Hz)
Cooling time	About 30 min. (from 300K to 77K)
Size (including cryostat)	50 mmϕ (diameter) x 400 mm (height)
Weight (including cryostat)	2.85 kg
Vibration at cold head	Less than 1.5 μm (at 77 K)
Compressor power	800 W (60Hz, air cooling)

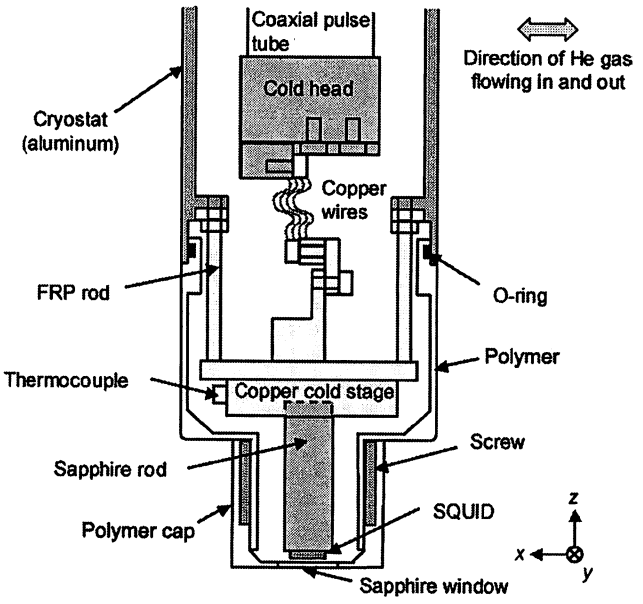

Fig. 3. Schematic cross-sectional view of the bottom part of the PTC and cryostat. By using a screw, the distance between SQUID and bottom of the cryostat could be as small as about 1 mm.

alternative copper cold stage was employed. Fig. 3 illustrates schematically the cross-sectional view of the bottom part of the PTC and cryostat. The copper cold stage was connected with the cold head by a bundle of flexible fine copper wires. The copper wires, through which the heat was transmitted, would suppress the vibration. The stage was fixed through fiber-reinforced plastic (FRP) rods to the inner wall of the cryostat. A sapphire rod with 15 mm in diameter and 50 mm in length was mounted on the cold stage. The SQUID was mounted atop the sapphire rod. By using a sapphire window 500-μm thick, the

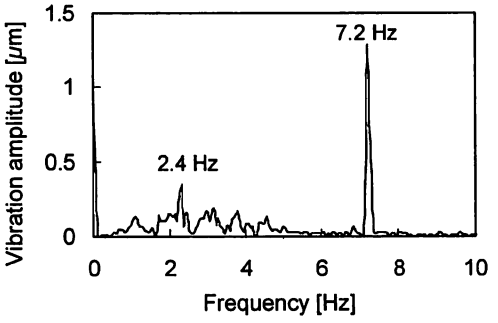

Fig. 4. Vibration at the cold stage in the x-direction measured using an accelerometer. The x-direction corresponds to the direction of He gas flowing in and out of the cryocooler as shown in Fig. 3. The oscillation frequency of the cryocooler was 2.4 Hz.

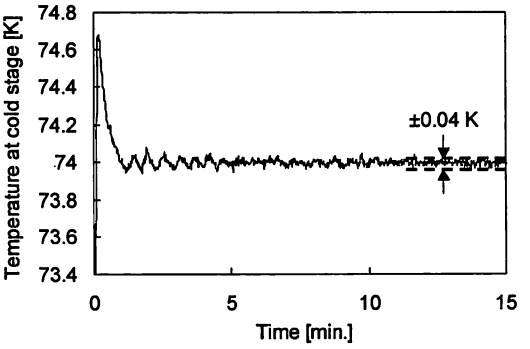

Fig. 5. Temperature at the cold stage as a function of time with temperature control. The temperature at the cold stage was set at 74 K. The initial temperature was set at 72.5 K by controlling the amount of He gas.

distance between the SQUID and the bottom of the cryostat could be as small as about 1 mm. Thermocouples were attached to the sidewalls of the cold head and the cold stage to monitor temperature.

The amplitudes of the vibration at the cold stage in the x, y, and z-directions—see Fig. 3—were measured using an accelerometer. Largest peak of 1.3 μm at 7.2 Hz (the third harmonic of the oscillation frequency) appeared at the cold stage in the x-direction, which corresponds to the direction of He gas flowing in and out of the cryocooler. The gas flow and the structure of the SQUID mount stage, which was supported by the FRP rods, may cause a larger vibration at 7.2 Hz than at 2.4 Hz. Fig. 4 shows the vibration measured at the cold stage in the x-direction.

The temperature of the cryocooler was primarily controlled by changing the amount of the coolant. For more precise temperature control, a proportional integral derivative (PID) temperature controller (Lakeshore 331) and sheet heaters were employed. Two heaters were wound around the cold stage in opposite directions in order to cancel magnetic noise generated by the heaters. It took less than 1 h to cool the SQUID from 300 K down to about 73 K and to stabilize the temperature at 74 K. The temperature of 74 K was selected because the SQUID gradiometer at 74 K is more sensitive than at 77 K. Fig. 5 shows temperature as a function of time. In this measurement, the initial temperature at the cold stage was set at about 72.5 K by controlling the amount of the coolant, and then the temperature of the stage was controlled to be stabilized at 74 K by the PID temperature controller. It took only 5 min for the temperature oscillation to be greatly reduced. The final temperature deviation was less than ±0.04 K.

D. Active Magnetic Shielding

The major problem encountered when the SQUID is moved quickly in an ambient field, is that the SQUID will unlock due to coupled flux noise that exceeds the slew rate. In order to solve this problem, we developed an active magnetic shielding technique with a simple compensation coil and feedback circuit including a narrow bandwidth elimination filter (BEF). In this scheme, the SQUID output caused by flux noise due to SQUID motion is negatively fed back to the compensation coil wound

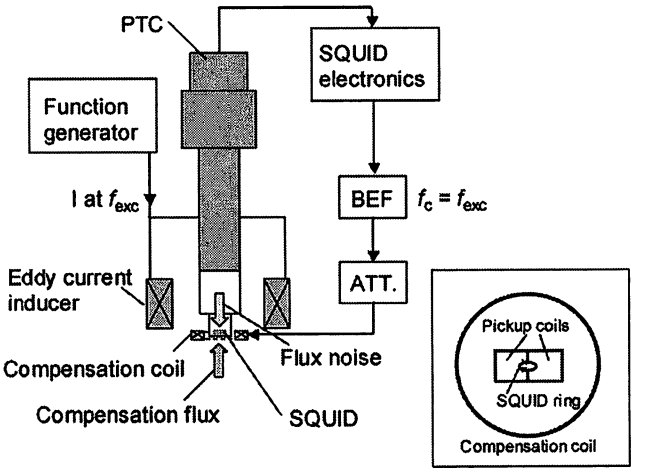

Fig. 6. Schematic diagram of the feedback circuit for the active magnetic shielding technique. The BEF was inserted in the circuit in order to cut off the components around the excitation field frequency f_{exc}. The inset shows the configuration of the SQUID gradiometer and the compensation coil.

just below the SQUID. The compensation coil generates a compensating magnetic flux, which actively cancels the magnetic flux coupled to the SQUID. Fig. 6 shows the schematic diagram of the feedback circuit used in the active magnetic shielding technique. We carefully aligned centers of both the compensation coil and the SQUID gradiometer, in order to prevent the compensation flux from affecting the differential pickup coils—see inset in Fig. 6. With this arrangement, uniform flux noise coupled to the SQUID ring is directly cancelled by the compensation flux. Concerning the field noise associated with the gradient, screening current due to the gradient field noise is directly coupled to the SQUID ring. Therefore, gradient field noise, which couples to the SQUID ring as flux noise, is indirectly cancelled by the compensation flux at the SQUID ring. In this system, a five-turn coil with a diameter of 20 mm was used as a compensation coil.

The narrow width BEF was inserted in the feedback circuit in order to cut off components in the region of an arbitrary frequency that was selectively used as the excitation field for flux compensation. The center of the cut-off frequency, f_c, of the BEF was set at the excitation frequency, f_{exc}. In this system,

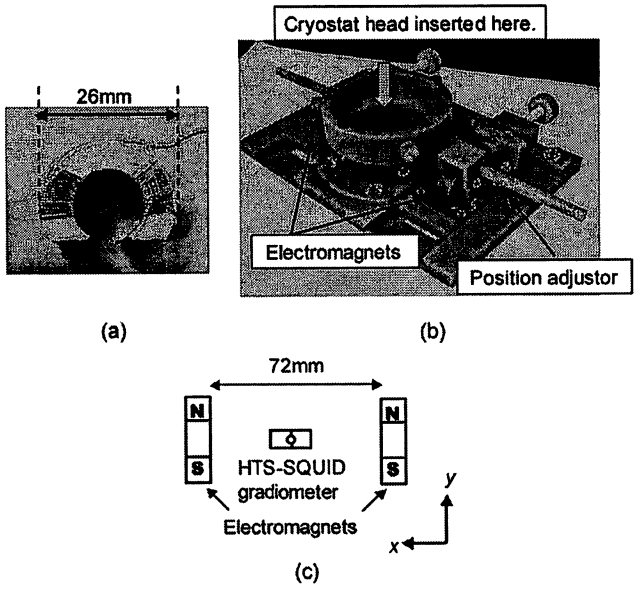

Fig. 7. (a) C-shaped ferrite core used in the electromagnet. Each has a 40-turn coil. (b) Eddy-current inducer. Position adjuster for the electromagnets was made of polymeric material. (c) Configuration of two electromagnets and SQUID gradiometer. Positions of the two electromagnets were carefully adjusted near the SQUID by using a position adjuster prior to measurement.

the BEF functions as a notch filter. Thus, the signal at the excitation frequency is not compensated, and magnetic noise except that near the excitation frequency is actively shielded.

E. Arm and XY Scanner

An aluminum arm was fixed to the electric XY slider as shown in Fig. 1(b). The cryostat integrated with the cryocooler was set on one end of the arm. A counterweight was set on the opposite end for balance. The XY scanner was controlled by means of a PC. The scanner had a spatial resolution of 10 μm, and could move at a maximum speed of 32 mm/s. The movable range of the scanner was 200 mm × 300 mm in the xy-plane. In order to suppress electric interference from the scanner, the cryostat was electrically isolated from the arm.

F. Eddy-Current Inducer

We employed two identical electromagnets with C-shaped ferrite cores, with each 40-turn coil serving as an eddy-current inducer. The ferrite cores were used to induce sufficient eddy current not only in metals, but also in the relatively much lower (one to three orders of magnitude) electrical conductivity of carbon-fiber composites. The size of the ferrites is shown in Fig. 7(a). A polymer position adjuster was made to adjust the positions of the two electromagnets, as shown in Fig. 7(b). The electromagnets were placed with bare ends perpendicular to the z-axis. Two electromagnets were placed in parallel on both sides of the SQUID to maintain symmetry of the generated excitation field as shown in Fig. 7(c). The bare ends of the electromagnets were leveled with the bottom of the cryostat. The positions of the two electromagnets were carefully adjusted by using the position adjuster prior to measurements, in order to minimize the excitation field coupled to the SQUID. The excitation field

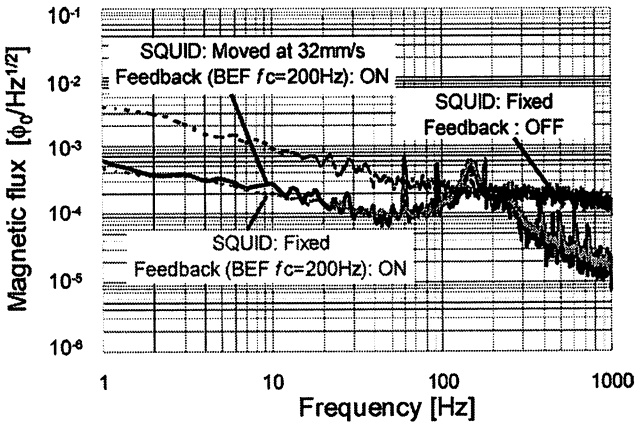

Fig. 8. Magnetic flux noise is shown during motion of the SQUID at 32 mm/s. In the feedback circuit, the center of the cutoff frequency, f_c, of the BEF was set at 200 Hz. For comparison, the noise for a fixed SQUID with and without a feedback circuit is shown together.

distribution generated by a C-shaped electromagnet is approximately identical to that generated by a double-D coil [12].

III. Performance of the System

A. System Noise During Motion of SQUID

The noise of the system during motion of the SQUID between 8 mm/s and 32 mm/s was measured. Fig. 8 shows typical measured system noise during motion of the SQUID at 32 mm/s using the BEF, which cut off components at about 200 Hz in the feedback circuit. Noise for a fixed sensor with and without the feedback circuit is presented in the figure for comparison. With the feedback circuit ON (the lower two sets of data), magnetic noise except around 200 Hz is well suppressed, compared to a fixed SQUID without a feedback circuit (the upper set of data). In addition, the noise spectrum during motion was approximately identical to that for the fixed SQUID with the feedback circuit operational. The noise level at 200 Hz during motion was almost the same as that for the fixed SQUID without a feedback circuit. Unlocking of the FLL circuit did not occur during all motion-based noise measurements. The peak noise observed at about 150 Hz with feedback activated may be due to a phase shift in the BEF.

B. Application to Carbon-Fiber Composites

To investigate the performance of the system, C/C plates were prepared as specimens. The C/Cs were the cross-ply laminated two-dimensional (2-D) type with symmetric fiber orientation $[0/90/45/-45]_s$. The fiber volume fill factor was 50%. The size of the plate specimen was 136-mm wide, 240-mm long and 10-mm thick. One specimen had an artificial slot 2-mm wide, 20-mm long, and 5-mm deep at the center of a broad plane surface.

The fixed slotted specimens were scanned in two dimensions by the mobile SQUID NDE system. Sinusoidal current of 140 mA at 270 Hz was applied to the electromagnets in parallel, generating a magnetic field of about 0.35 mT at the bare ends of the electromagnets. The lift-off distance (between SQUID and specimen surface) was set at about 2 mm. The sampling

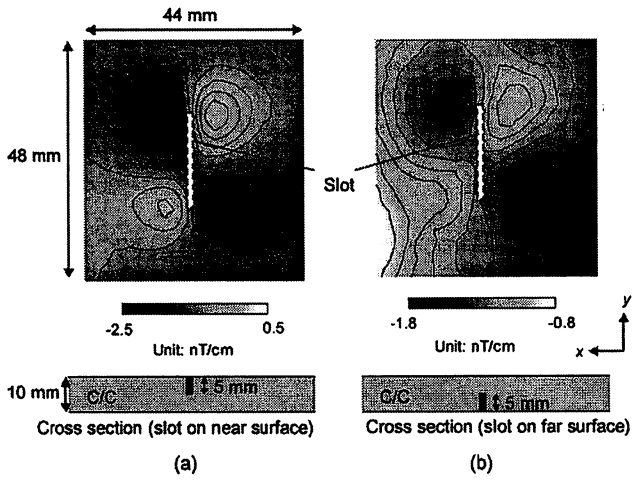

Fig. 9. Two-dimensional scanning results. (a) On C/C plate with a slot on the near surface. (b) On C/C plate with a slot on the far surface. Quadrupole signals appeared around each slot. The cross sections of the specimens are drawn below the results. During the measurements, the SQUID gradiometer was moved at 8 mm/s with a space interval of 2 mm in the x and y-directions.

space interval was 2 mm in both the x and y-directions. An area of 44 mm in the x-direction and 48 mm in the y-direction about the slot was scanned. The SQUID was used to measure the field gradient $\mathrm{d}B_z/\mathrm{d}x$. At first, the specimen was scanned while the slot was on the near surface, and then it was scanned with the slot being on the far surface. The SQUID was moved at 8 mm/s during these measurements.

Fig. 9(a) and (b) show the 2-D scanning results on the C/C plate specimens for a near surface slot and for a far surface slot, respectively. These figures show the contour map of the distribution of in-phase components of the lock-in detector for $\mathrm{d}B_z/\mathrm{d}x$. In each figure, quadrupole signals were observed around the slot due to the arrangement of the SQUID gradiometer and eddy-current inducer. In Fig. 9(b), although the signal amplitude decreased due to the increase in distance between the SQUID and the back surface slot, quadrupole signals due to the hidden slot in the C/C plate were easily observed by the mobile sensor system.

Multi-layered C/C specimens also were examined. The specimens were double-layered C/C plate specimens with a total thickness of 20 mm. Fig. 10(a) shows the cross-sectional views of the double-layered specimens with slots in the second layer of the C/Cs. The specimens had a hidden slot with depths of 10 mm and 15 mm, respectively. The same types of C/C plates, but without slots as noted above, were stacked over the C/C plate with the slot. These two double-layered specimens also were scanned by the NDE system with the same measurement setting and parameters. In both cases, the quadrupole signals also were observed around the slots with the same resolution as that seen in the Fig. 9 data. Fig. 10(b) shows the relation between the signal peak-to-peak amplitude and the slot depth obtained by scanning the single- and double-layered C/C specimens. We defined the signal peak-to-peak amplitude as the difference in signal amplitude between the maximum peak and the minimum peak in the quadrupole signals. As shown in the figure, the signal peak amplitude decreases roughly exponentially with increasing slot depth. The frequency range of the electronics limited the signal-to-noise ratio and the detectable slot depth. However,

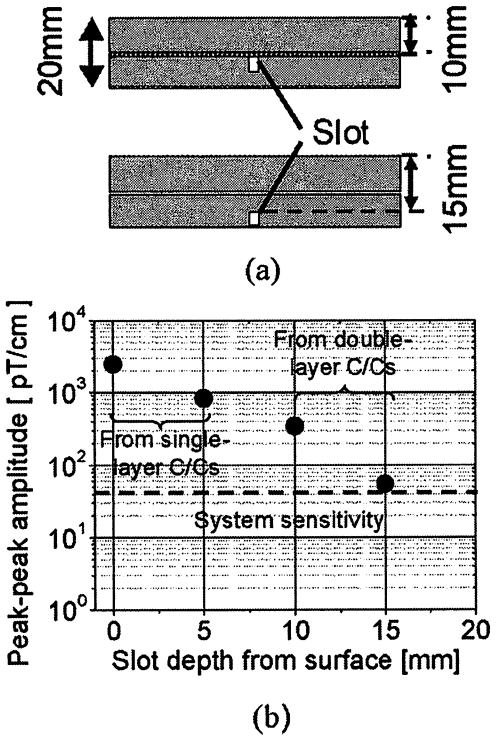

Fig. 10. (a) Cross-sectional views of the double-layered C/C specimens. The size of the C/C plate with the slot was the same as that shown in the Fig. 9. (b) The signal peak-to-peak amplitude as a function of the slot depth from the surface.

since the penetration depth of the C/Cs is much larger than for metals, using higher excitation fields with one to orders of magnitude higher frequency, should improve the detectable depth limit up to about 30 mm. Actually, a detectable depth of 30 mm will be required for safety inspections, e.g., on rocket nozzles, in which C/Cs with thickness of over 30 mm are often used.

IV. Conclusion

A cryocooler-based mobile SQUID NDE system was constructed by employing an active magnetic shielding technique with a simple compensation coil and feedback circuit including a narrow band BEF. Flux noise caused by moving a SQUID (at least) up to 32 mm/s was well suppressed. Unlocking of the FLL circuit or a significant increase in the noise did not occur during the motion. Detection of slots in single and double-layered C/C plates in an ambient field by moving the HTS SQUID gradiometer was demonstrated as a test of the performance of the system. The quadrupole signal responses due to the hidden slots with depths up to 15 mm in C/C specimens could be observed by the mobile sensor system for fixed specimens. The results are encouraging for the possible application of SQUID NDE to *in situ* large-scale structures such as aircraft and space shuttles that are comprised (to some extent) of carbon-fiber composites.

Acknowledgment

The authors would like to thank Dr. N. Kasai, AIST, Japan, for the helpful discussions on this research, Dr. H. Hatta, JAXA,

Japan, for providing them with the 2-D-C/Cs specimens, and Dr. H. Weinstock, AFOSR, for his kind suggestions.

REFERENCES

[1] Y. Tavrin, H.-J. Krause, W. Wolf, V. Glyantsev, J. Schubert, W. Zander, and H. Bousack, "Eddy current technique with high temperature SQUID for nondestructive evaluation of nonmagnetic metallic structures," *Cryogenics*, vol. 36, pp. 83–86, 1996.

[2] C. Carr, D. M. McKirdy, E. J. Romans, G. B. Donaldson, and A. Cochran, "Electromagnetic nondestructive evalation: moving HTS SQUID's, inducing field nulling and dual frequency measurements," *IEEE Trans. Appl. Supercond.*, vol. 7, no. 2, pp. 3275–3278, Jun. 1997.

[3] R. Hohmann, M. Maus, D. Lomparski, M. Geuneklee, Y. Zhang, H.-J. Krause, H. Bousack, and A. I. Braginski, "Aircraft wheel testing with machine-cooled HTS SQUID gradiometer system," *IEEE Trans. Appl. Supercond.*, vol. 9, no. 2, pp. 3801–3804, Jun. 1999.

[4] Y. Tavrin, M. Siegel, and J. Hinken, "Standard method for detection of magnetic defects in aircraft engine discs using a HTS SQUID gradiometer," *IEEE Trans. Appl. Supercond.*, vol. 9, no. 2, pp. 3809–3812, Jun. 1999.

[5] N. Kasai, D. Suzuki, H. Takashima, M. Koyanagi, and Y. Hatsukade, "HTS-dcSQUID gradiometer for nondestructive evaluation," *IEEE Trans. Appl. Supercond.*, vol. 9, no. 2, pp. 4393–4396, Jun. 1999.

[6] A. Ruosi, M. Valentino, G. Peluso, and G. Pepe, "Analysis of low-velocity impact damage in reinforced carbon fiber composites by HTS-dc-SQUID magnetometer," *IEEE Trans. Appl. Supercond.*, vol. 11, no. 1, pp. 1172–1175, Mar. 2001.

[7] C. Carr, D. Graham, J. C. Macfarlane, and G. B. Donaldson, "SQUID-based nondestructive evaluation of carbon fiber reinforced polymer," *IEEE Trans. Appl. Supercond.*, vol. 13, no. 2, pp. 196–199, Jun. 2003.

[8] Y. Hatsukade, M. S. Aly-Hassan, N. Kasai, H. Takashima, H. Hatta, and A. Ishiyama, "SQUID-NDE method on damaged area and damage amount of defects in composite materials," *IEEE Trans. Appl. Supercond.*, vol. 13, no. 2, pp. 207–210, Jun. 2003.

[9] Y. Bar-Cohen. (1999) In-Service NDE of Aerospace Structures—Emerging Technologies and Challenges at the End of the 2nd Millennium. NDT.net. [Online] Available: http://www.ndt.net/article/v04n09/bcohen/bcohen.htm

[10] H.-J. Krause, W. Wolf, G. Glaas, E. Zimmermann, M. I. Faley, G. Sawade, R. Mattheus, G. Neudert, U. Gampe, and J. Krieger, "SQUID array for magnetic inspection of prestressed concrete bridge," *Physica C*, vol. C–368, pp. 91–95, 2001.

[11] D. F. He, M. Daibo, and M. Yoshizawa, "Mobile HTS rf SQUID magnetometer," *IEEE Trans. Appl. Supercond.*, vol. 13, no. 2, pp. 200–202, Jun. 2003.

[12] A. Ruosi, G. Pepe, G. Peluso, M. Valentino, and V. Monebhurrun, "Experimental and numerical results of electromagnetic nondestructive testing with HTc SQUIDs," *IEEE Trans. Appl. Supercond.*, vol. 9, no. 2, pp. 3499–3502, Jun. 1999.